https://doi.org/10.5194/gmd-2022-146
Preprint. Discussion started: 11 July 2022

Geoscientific Model Development
Discussions

Data-driven Global Subseasonal Forecast Model (GSFM v1.0) for intraseasonal oscillation components

Chuhan Lu[1], Dingan Huang[1], Yichen Shen[1], and Fei Xin[2]

[1] Key Laboratory of Meteorological Disaster of Ministry of Education/Collaborative Innovation Center on Forecast and Evaluation of Meteorological Disasters, Nanjing University of Information Science & Technology, China

[2] Shanghai Climate Center, China

Correspondence: Chuhan Lu (luchuhan@nuist.edu.cn)

Abstract As a challenge in the construction of a "seamless forecast" system, improving the prediction skills of subseasonal forecasts is a key issue for meteorologists. In view of the evolution characteristics of numerical models and recent deep learning models for subseasonal forecasts, as forecast times increase, forecast results tend to become intraseasonal low-frequency components, which are essential to the change in general circulation on the subseasonal timescale as well as persistent extreme weather. In this paper, the Global Subseasonal Forecast Model (GSFM v1.0) first extracted the intraseasonal oscillation (ISO) components of atmospheric signals and used an improved deep learning model (SE-ResNet) to train and predict the ISO components of geopotential height at 500 hPa (Z500) and temperature at 850 hPa (T850). The results show that the 10-30 day prediction performance of the model used in this paper is better than that of the model trained directly with original data. Compared with other models/methods, the SE-ResNet model has a good ability to depict the subseasonal evolution of the ISO components of Z500 and T850. In particular, although the CFSv2 results have a better prediction performance through 10 days, the SE-ResNet model is substantially superior to CFSv2 through 10-30 day, especially in the middle and high latitudes. The SE-ResNet model also has a better effect in predicting 3-8 planetary waves, which leads to the difference in model prediction performance in extratropical areas. A case study shows that the SE-ResNet model depicted the phase change and propagation characteristics of planetary waves well. Thus, the application of data-driven subseasonal forecasts of atmospheric ISO components may shed light on improving the skill of seasonal forecasts.

1. Introduction

In the meteorological department, forecasts on the 10-30 day timescale lie between 0-10 day short- and mid-term weather forecasts and monthly scale short-term climate forecasts, which are called subseasonal or extended-range forecasts and are a crucial link in the construction of seamless and refined forecasting and prediction systems (Jin et al., 2019). However, it is also difficult to construct a "seamless forecast" system

https://doi.org/10.5194/gmd-2022-146
Preprint. Discussion started: 11 July 2022

(Hoskins, 2013).

Subseasonal forecasts lack predictability due to the chaotic nature of the atmosphere (Mayer et al., 2021) and thus have a rather limited predictive signal over subseasonal timescales (Srinivasan et al., 2021). To accelerate the research progress of subseasonal forecasting and bridge the timescale gap between synoptic-scale forecasting and short-term climate forecasting, the World Weather Research Programme (WWRP) and the World Climate Research Programme (WCRP) jointly launched a 5-year research programme called the Subseasonal to Seasonal (S2S) Prediction research project to improve the ability of extended-range forecasting and the understanding of the sources of subseasonal to seasonal predictability (Vitart et al., 2017). To address this academic challenge, meteorologists have made various attempts and studies on subseasonal forecasting, resulting in remarkable progress. The Madden-Julian Oscillation (MJO) is the most important source of forecasting skills on the subseasonal timescale (Robertson et al.,2015), and an empirical model of spring precipitation forecasts in southern China on the subseasonal timescale was established by Li et al. (2016) using the spatiotemporal information of MJO as a predictor. In addition, Zhu et al. (2017) constructed spatial-temporal projection models (STPM) to carry out real-time subseasonal forecasts for tropical cyclones over the western North Pacific.

Although the timescale of the subseasonal forecast exceeds the theoretical upper limit of the daily weather forecast, atmospheric movement still has predictable components (Zhu et al.,2014), and the predictability of atmospheric movement is related to the spatial-temporal scale (Zhang et al., 2019). Hsu et al. (2015) developed a set of methods to extract low-frequency signals from the atmosphere for 10-60 day without using bandpass filters, and the developed STPM showed good performance in subseasonal precipitation forecasting in South China. Wang et al. (2014), by extracting the predictable component on the subseasonal timescale and referring to the conditionally nonlinear optimal perturbation (CNOP) correlation algorithm, developed a practical method and prediction technology for extracting the predictable components in numerical models.

Weather and climate systems are typically nonlinear systems, and the characteristics of high dimensionality, large quantity and complexity of meteorological data make it difficult to forecast accurately. The ability of artificial intelligence technology to effectively learn and capture features in massive data has been widely applied in various fields. Machine learning, especially deep learning technology, has also been widely used in meteorological research and business fields in recent years, from the automatic recognition of tropical cyclones (Hong et al., 2017), extratropical cyclones (Lu et al., 2020) and fronts (Lagerquist et al., 2019; Lagerquist et al., 2020) to the prediction techniques of nowcasting (Shi et al., 2015; Ravuri et al., 2021), weather forecasting (Weyn et al., 2019) and ENSO forecasting (Ham et al., 2019). For example, Song et al. (2019) developed the SE-ResUNet model for the prediction of precipitation near Beijing and achieved better results than traditional weather forecasts. Sønderby et

https://doi.org/10.5194/gmd-2022-146
Preprint. Discussion started: 11 July 2022

al. (2020) evaluated the performance of MetNet under different precipitation thresholds and found that MetNet is superior to numerical weather forecasting to some extent. Rasp and Thuerey (2021) used the ResNet model to predict geopotential height, temperature and precipitation in the next 5 days and obtained more reliable results.

Machine learning has made considerable progress in weather-scale prediction, but further research on subseasonal-scale prediction is still needed. Machine learning can provide a potential approach to the development of S2S prediction systems with significantly reduced computational costs (Weyn et al., 2021). Residual structure has an excellent feature extraction ability (Jin et al., 2021), so we attempt to apply this structure to the field of subseasonal prediction. However, with the extension of forecast time, the prediction results will gradually smoothen (Rasp et al., 2020) and tend to become low-frequency signals of the atmosphere (Weyn et al., 2021). In fact, in the deep learning process of subseasonal forecasts, as the loss function mostly adopts spatial root mean square error, the prediction result will tend to be “fuzzy” as the forecast time increases (Mathieu et al., 2015), showing the low-frequency or low degree of freedom characteristics of atmospheric circulation during the subseasonal forecast process. In view of this “low-frequency” feature, can we reduce the degrees of freedom of the atmospheric elements in advance by extracting the intraseasonal oscillation signals from them to focus the learning object of the learning model, in order to improve the learning ability of the model and the forecast performance? In fact, weather and climate systems are complex systems composed of multiscale interactions of small-scale, high-frequency and low-frequency evolution. Reliable representation of multiscale characteristics is one of the important conditions for the development of high-performance weather/climate prediction models (Slingo et al., 2008). Spectral analysis (extraction of different components) provides novel ways of incorporating the multiscale properties of weather and climate systems in machine learning (Kashinath et al. 2021). For example, Wu et al. (2020) developed a generative adversarial network (GAN) partial differential solution model to describe Rayleigh-Bénard convective activity by enhancing covariance constraints and pointed out that these constraint pairs help preserve and highlight the physical characteristics of the corresponding spectrum. Mohan et al. (2020) used wavelet transformation to predict turbulence by constructing wavelet coefficients based on physical features.

In addition, since multifactor predictors can be input into the forecast model, the contributions of evolution among different factors to the forecast may be different. Can a self-attention mechanism such as squeeze-and-excitation (Hu et al., 2017) be introduced to optimize the contribution of different elements (channels) to the model? Therefore, this study attempted to predict the ISO components of Z500 and T850 in the next 1-30 day by using an improved deep learning model (SE-ResNet, which combines the self-attention mechanism and the ResNet prediction model). The SE-ResNet model was quantitatively evaluated by comparing the prediction results with those of the CFSv2 and ResNet models against ERA5 data.

https://doi.org/10.5194/gmd-2022-146
Preprint. Discussion started: 11 July 2022

2 Methods

2.1 Filtering method

To allow the model to be applicable for real-time forecasting, this paper uses the filtering method proposed by Hsu et al. (2015) to extract atmospheric signals over 10-30 day. This method can be divided into three steps. (1) Remove the slow-varying climatologic annual circle by subtracting the climatologic 90-day low-pass filtered components from the raw data. (2) Remove other ISO signals by subtracting the last 15-day running mean. (3) Remove the synoptic scale components by taking a 5-day running mean.

To have comparable forecasting, the results are defined as the results of the ISO components predicted by the model plus the climatology of the elemental fields for the corresponding date calculated using data from 1981 to 2010.

2.2 Forecast model

The forecast model used in this paper is developed based on the ResNet model designed by Rasp et al. (2020) and has been further improved according to the prediction objectives. The specific model structure is shown in Fig. 1. The ResNet model and SE-ResNet model mentioned in this paper both contain 17 residual blocks, which consist of two convolution blocks. The convolution block is defined as a 2D convolution layer, an activation function layer, a batch normalization layer and a dropout layer. All convolutions are padded periodically in the longitudinal direction but zero in the latitudinal direction. The SE-ResNet model for this study is a further improvement by the model above. Both models have a similar structure and use the same convolution block, but in the residual block of the SE-ResNet model, a squeeze-and-excitation block is added, which works as a self-attention mechanism. When there are multiple elements input into the model, the squeeze-and-excitation block can choose the importance of each channel through the squeeze and excitation operations, and the weight coefficient is put on each channel by the scale operation to complete the recalibration of the importance of the original channel (Hu et al., 2017). The residual block obtains the final output by adding the output of the squeeze-and-excitation block and the input of the residual block. In addition, since this method is a point-to-point forecast, there is a corresponding forecast model for each forecast lead time, so the prediction task of 1-30 day is completed by 30 models representing different forecast times. The parameters in training the SE-ResNet model are set as follows. The initial learning rate is set to 0.5×10^{-4}, which will be reduced by a factor of 5 once the validation loss has not decreased for 2 epochs. The number of residual blocks is 17. Each residual block contains two convolution blocks with 128 channels. The convolution kernel size is 3. Weight decay is 0.01 used for all layers. The activation function is LeakyReLU. Dropout is set to 0.3. Model training data are provided by the WeatherBench challenge. A detailed description can be found in studies of Rasp et al. (2020), and the data set mainly contains ERA5 data from 1979 to 2018, and the horizontal resolution of the data set used in this paper is 5.625°×5.625°.

https://doi.org/10.5194/gmd-2022-146
Preprint. Discussion started: 11 July 2022

Geoscientific Model Development
Discussions
Open Access
EGU

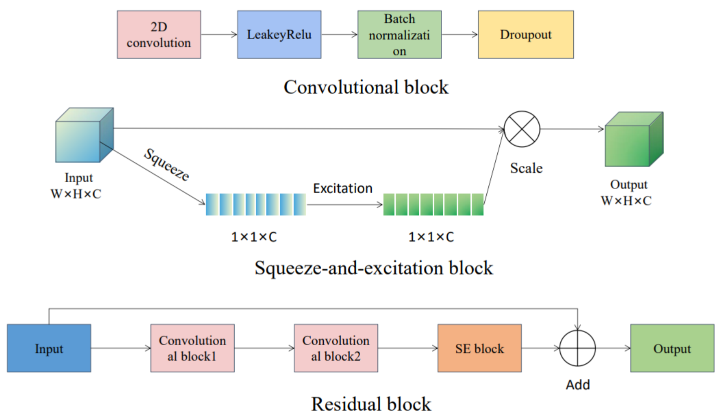

Figure 1. Schematic diagram of the model structure

2.3 Forecast effect evaluation methods

To evaluate the forecast results of the model, the area-weighted root mean squared error (RMSE) is defined as

$$RMSE = \frac{1}{N_{forecasts}} \sum_{i}^{N_{forecasts}} \sqrt{\frac{1}{N_{lat} N_{lon}} \sum_{j}^{N_{lat}} \sum_{k}^{N_{lon}} L(j)(f_{i,j,k} - t_{i,j,k})^2} \tag{1}$$

where f is the prediction result of the model, and t is the ERA5 data of the corresponding time. The smaller the RMSE value is, the better the prediction result of the model is. The abnormal correlation coefficient (ACC) is defined as

$$ACC = \frac{\sum_{i,j,k} L(j) f'_{i,j,k} t'_{i,j,k}}{\sqrt{\sum_{i,j,k} L(j) f'^2_{i,j,k} \sum_{i,j,k} L(j) t'^2_{i,j,k}}} \times 100 \tag{2}$$

where the symbol ' represents the difference to the climatology, $L(j)$ is the weight factor when latitude is j, and $L(j)$ is defined as

$$L(j) = \frac{\cos(lat(j))}{\frac{1}{N_{lat}} \sum_{j}^{N_{lat}} \cos(lat(j))} \tag{3}$$

ACC can represent the similarity of two fields. The closer the absolute value of ACC is to 100, the more similar the two fields are.

3. Model forecast results

3.1 Prediction case analysis: original data vs. ISO component

This paper mainly focuses on the 10-30 day forecast ability of ISO components. To show the importance of ISO components in actual atmospheric changes and the forecast ability of ISO components of the forecast process, Figure 2 compares the zonal deviation of ERA5 and predicted Z500 and its ISO components during 7-19 November

https://doi.org/10.5194/gmd-2022-146
Preprint. Discussion started: 11 July 2022

2017. According to the variations in the ERA5 original field and ERA5 ISO component field over time (Fig. 2a and 2b), the ERA5 ISO components reasonably reflect the main trough-ridge system (Rossby wave) and its characteristics of amplitude and movement variation over time of the original Z500 in the middle and high latitudes of the Northern Hemisphere, including troughs along the western coast of Europe, East Asia, the Gulf of Alaska, and northeastern Canada, as well as ridges in the midlatitude North Atlantic, Urals, and south of the Aleutian Islands. Although the amplitudes of the ISO components are slightly smaller for these weather fluctuations, the mean variance contribution is 26.67 %, indicating that the ISO components are of paramount importance to actual atmospheric change. In fact, the ISO components are good indicators of large-scale persistent circulation systems and their associated extreme weather and climate events (e.g., Qi et al. 2019).

Predictions at forecast lead times of 10-22 day based on the original and ISO components can both well reflect the variation characteristic of the deep trough in the East Asian region as well as in northeast Canada. The variation characteristics of the shallow trough in the gulf of Alaska and the ridges on the west coast of North America and northwest Eurasia can also be reasonably reflected, but the prediction results are weaker in oscillation variation and smoother in streamlines than the midlatitude atmospheric fluctuations described by the ERA5 ISO components (Fig. 2c, 2d). The global mean RMSE of the prediction driven by ISO components for the next 10-22 day is 541.20 $m^2\ s^{-2}$, which is notably better than that of the CFSv2 prediction for the same period (RMSE: 563.32 $m^2\ s^{-2}$). Interestingly, the model prediction results of Z500 driven by original (unfiltered) data have a similar spatial form to that predicted using ISO components, showing a distinct "low-frequency" (smoothened) feature. Furthermore, in this case, the Z500 values predicted by the ISO components are closer to the ERA5 ISO components, with a mean RMSE of 575.96 ($m^2\ s^{-2}$). Similarly, the T850 values predicted by the ISO components are in better agreement with the ERA5 ISO components (Fig. A1). The mean RMSE for the ISO components at 10-22 day is 2.13 (K), which is significantly lower than the prediction driven by the original data (2.26 K). This may be because the degrees of freedom and complexity of the ISO components are lower than those of the original variables, which could lead to the learning ability of the model based on ISO components being better than that of the model driven by the original data.

https://doi.org/10.5194/gmd-2022-146
Preprint. Discussion started: 11 July 2022

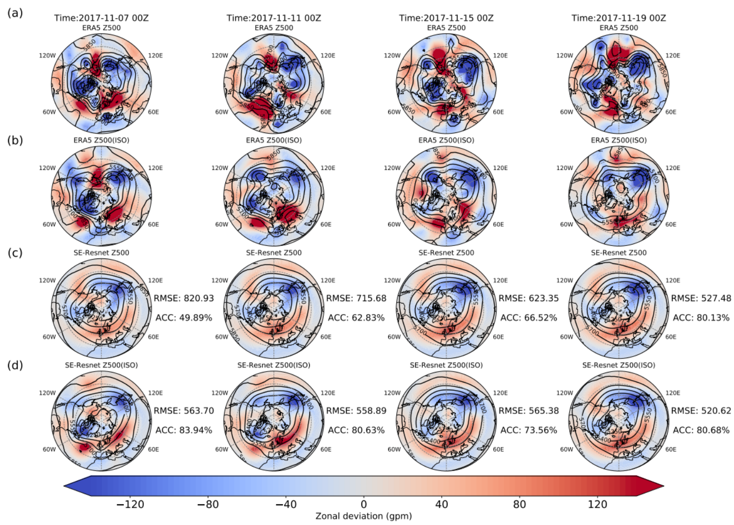

Figure 2. Result and zonal deviation comparison of model predictions for Z500 (unit: gpm) in the Northern Hemisphere (20°-90° N, 180° W-180° E). Forecast lead times from left to right are 10 days, 14 days, 18 days and 22 days, respectively.

3.2 Overall evaluation of the model

To reflect the long-term overall prediction result of the model, Figure 3 presents the RMSE of the model's prediction results for the global average Z500 and T850 ISO components at forecast lead times of 10-30 day in 2017-2018 (a total of 2920 initial conditions, i.e., 2920 samples). For the ISO component forecast, the RMSE values of CFSv2, ResNet and SE-ResNet results of global Z500 all increase with the forecast lead times. The increase rate is larger through 20 days and flattens after that, with a smaller decrease rate with time. ResNet and SE-ResNet are better than climatological forecast (mean RMSE: 578 m^2 s^{-2}) and persistence forecast (the worst prediction, mean RMSE: 859 m^2 s^{-2}) over the 10-30 day forecast lead times. It is noteworthy that the average RMSE of the CFSv2 model is larger than those of the ResNet model and the SE-ResNet model when the forecast lead times are more than 12 days, indicating that although the prediction of global atmospheric circulation and its ISO components over 10 days based on the dynamic seasonal climate prediction system still has a great advantage, the prediction ability of the subseasonal atmospheric circulation beyond 12 days is weaker than those of the data-driven ResNet model and the SE-ResNet model. Compared with the climatological forecast, the CFSv2 model has lower prediction skills after 16 days. Moreover, the average RMSE of the SE-ResNet model is 1.01 % lower than that of the ResNet model through lead times of 10-30 day. This is an improvement on the ResNet model because of the squeeze-and-excitation block, which optimizes the output based on the importance and weight of each factor when using multiple inputs.

As seen from the RMSE boxplot of ISO components of Z500 every 5 days (Fig. 3c), 75 % of the samples predicted by the deep learning model are below the

https://doi.org/10.5194/gmd-2022-146
Preprint. Discussion started: 11 July 2022

climatological forecast in 10-15 day, and more than 50 % of the samples predicted remain below the climatological forecast after that. The CFSv2 model predictions have 50 % of the samples higher than the climatological forecast in 16-20 day and beyond. The persistence forecast is the worst, with the RMSE of all the predicted samples being higher than the climatological forecast, and the RMSE of more than 75 % of the samples is above 1000 m^2 s^{-2}. Not surprisingly, the SE-ResNet model has the "best" inaccurate forecast case (RMSE: 647.34 m^2 s^{-2}), followed by the ResNet model, CFSv2 model, and persistence forecast. For the "best" accurate forecast case, SE-ResNet and ResNet are close, outperforming the CFSv2 model and persistence forecast beyond 16 days. On the other hand, the "best" accurate forecast case of each model is obtained from the 10-15 days CFSv2 model with an RMSE of 346.38 m^2 s^{-2}.

For the global average ISO components of T850, the prediction result of each model is similar to the ISO components of Z500. As shown in Fig. 3b, the SE-ResNet model is still the model with the highest forecasting skills, with an average RMSE 0.75 % lower than the ResNet model through forecast lead times of 10-30 day. Both the SE-ResNet model and ResNet model are superior to climatological forecasts, and their RMSE beyond 11 days of forecasting is significantly lower than that of the CFSv2 model, which is inferior to climatological forecasts beyond 14 days. In the RMSE boxplot of ISO components of T850 every 5 days (Fig. 3d), the overall prediction performance of SE-ResNet and ResNet outperform CFSv2 model and persistence forecast. The SE-ResNet model has the "best" inaccurate prediction case (RMSE: 2.68 K), followed by the ResNet model, CFSv2 model and persistence forecast. For the "best" accurate prediction case, the SE-ResNet, ResNet, and CFSv2 models are close, but the RMSE value of the CFSv2 model increases slightly beyond 21 days.

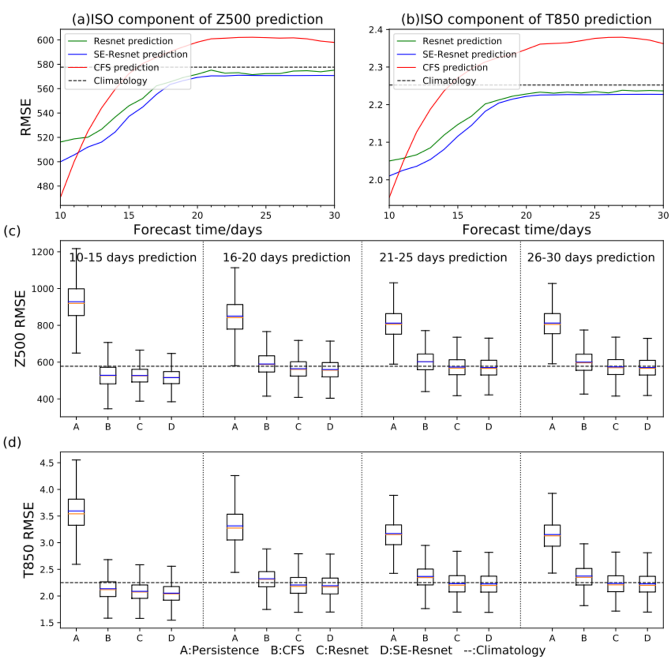

https://doi.org/10.5194/gmd-2022-146
Preprint. Discussion started: 11 July 2022

Figure 3. Mean RMSE of ISO components of model prediction varies with the forecast lead times for (a) Z500[m^2 s^{-2}], (b) T850[K] and the boxplot of RMSE every 5 days for (c) Z500[m^2 s^{-2}], (d) T850[K] evaluated against ERA5 data.

To quantitatively show the spatial similarity between the ISO components predicted by different models and the ERA5 ISO components, the sequence of the globally averaged ACC of the predicted ISO components for Z500 and T850 with forecast lead times is given in Fig. 4. The results are similar to the RMSE results analysis, and the ACC skills of the deep learning model are significantly superior to other models beyond 12 days. Among them, the spatial similarity between the predicted ISO components of the SE-ResNet model and the ERA5 ISO components is the highest, and the ACC of Z500 and T850 for 10-30 day is 72.90 % and 82.89 %, respectively. Unsurprisingly, its prediction result for 10-30 day ahead is higher than the climatological forecast. The ResNet model has the second highest ACC skills, with an averaged ACC of 72.19 % for Z500 and 82.59 % for T850 through 10-30 day. ACC corresponding to the Z500 and T850 ISO components predicted by CFSv2 is lower than the climatological forecast in approximately 17 and 15 days, respectively, and lower than the aforementioned two deep learning models beyond forecast lead times of 12 days, whose ACC of Z500 and T850 in 10-30 day is 70.11 % and 80.83 %, respectively. The ACC skills of the persistence forecast are the worst, with an average ACC of 47.48 % and 65.28 % for Z500 and T850 during 10-30 day, respectively.

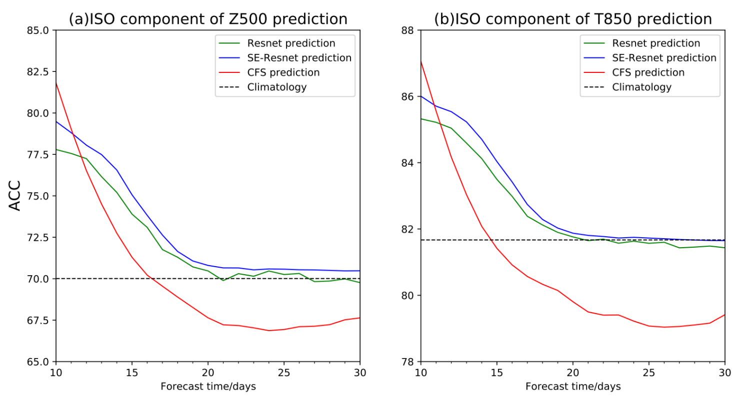

Figure 4. Mean ACC of ISO components of model prediction varies with the forecast lead times for (a) Z500 and (b) T850

From the perspective of the global average, the above section shows that the prediction ability of the SE-ResNet model is better than CFSv2 for the Z500 and T850 ISO components during 14-30 day. To further show the difference in the prediction effects of the two at different latitudes, Figure 5 demonstrates the difference between the zonally averaged RMSE of the prediction results of the CFSv2 and SE-ResNet models under different forecast lead times. The large RMSE difference between the two

https://doi.org/10.5194/gmd-2022-146
Preprint. Discussion started: 11 July 2022

models mainly occurs in the extratropical region of the two hemispheres, while the difference is relatively small in the tropical region. In general, CFSv2 has a large advantage in the prediction of the Z500 and T850 ISO components when the forecast lead time is less than 10 days. However, when the forecast lead time is more than 10 days, the prediction results of the SE-ResNet model are stably better than those of CFSv2, which is consistent with the analysis results of the global average (Fig. 3). Specifically, the RMSE predicted by the SE-ResNet model for Z500 (T850) is 28.71 $m^2\ s^{-2}$ (0.14 K) lower on average than CFSv2 in the 20-80° region when the forecast lead time is more than 10 days.

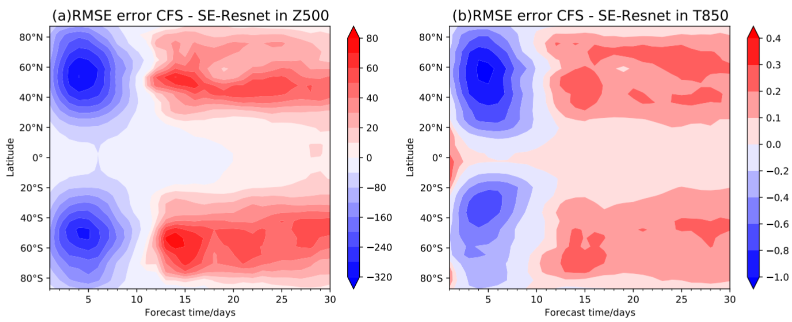

Figure 5. The difference in the zonally averaged RMSE of the CFSv2 and SE-ResNet models at different forecast lead times: (a) Z500[$m^2\ s^{-2}$], (b) T850[K]

Since planetary waves are the main drivers of atmospheric circulation at middle and high latitudes and regional weather/climate anomalies, the enhancement of planetary wave activity is closely related to long-term extreme climate events (e.g., Petoukhov et al., 2013; Screen and Simmonds, 2014), so the simulation difference between CFSv2 and SE-ResNet in the extratropical region may be due to the difference in the prediction skills of planetary waves. Figure 6a and 6b further show the RMSE and ACC of the CFSv2 and SE-ResNet models for planetary waves with wavenumbers of 3-8 in 30-70° N latitudes in the Northern Hemisphere compared with ERA5 data. It can be clearly seen that the SE-ResNet model has a good skill in the prediction of planetary waves with wavenumbers of 3-8 beyond 11 days. The average RMSE of the SE-ResNet model is 524.22 $m^2\ s^{-2}$ during the forecast lead times of 11-25 day, which is significantly lower than the climatology (551.39 $m^2\ s^{-2}$) and CFSv2 model (555.32 $m^2\ s^{-2}$). Compared with the CFSv2 model, the SE-ResNet model is 31.10 $m^2\ s^{-2}$ lower on average at 11-25 day, which is equivalent to the average zonal deviation of the two models shown in Fig. 5a, indicating that the difference in the prediction effect for extratropical Z500 is mainly due to the difference in prediction performance of the above two models for planetary waves. At the same time, the ACC results also show that the performance of the SE-ResNet model is higher than that of the climatology (82.29 %) during 11-25 day, while the CFSv2 model has low prediction skills beyond 16 days.

https://doi.org/10.5194/gmd-2022-146
Preprint. Discussion started: 11 July 2022

Geoscientific Model Development
Discussions
Open Access

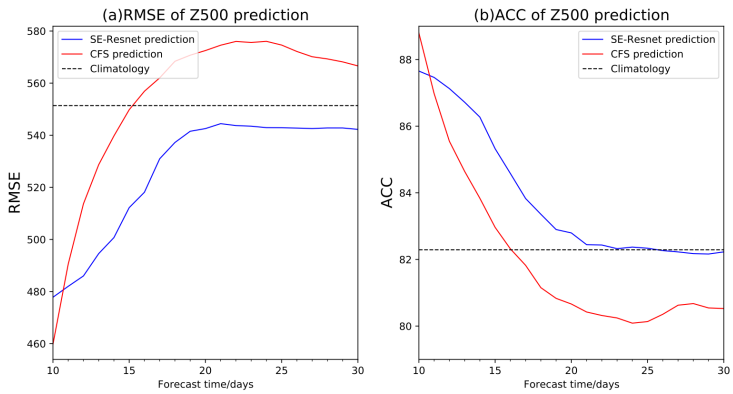

Figure 6. The prediction results of Z500 planetary waves (3-8 waves) at different forecast lead times: (a) RMSE[m^2 s^{-2}], (b) ACC.

3.3 Prediction and evaluation of the 500 hPa circulation situation in the Eurasian region

Focusing on the reliability of the 10-30 day forecast of regional upper-level circulation by different methods, the following section uses the Eurasian region as an example to give an individual case and their overall prediction performance. Figure 7 first shows the Z500 ISO components of a cold wave weather process in Eurasia from 3-9 December 2018, and the difference in ERA5 ground 2 m temperature between the schematic time and 12 UTC on 2 December 2018. This event was a continuous large-scale cold wave affecting East Asia, with the cooling area mainly concentrated in eastern China, the Korean Peninsula and Japan, and the local temperature dropped up to 16.09 K (24.91 K) within 24 (72) hours. During this process, the characteristics of planetary wave activity were obvious and were mainly caused by the continuous maintenance and strengthening of the blocking high near the Ural Mountains, leading to the deepening and development of the downstream East Asian trough. Meanwhile, along with the continuous eastward movement of the low trough in Central and Western Europe, a large amount of cold air from the northwest entered East Asia, resulting in widespread and persistent cooling. According to the predicted results, the three models reflect the phase and propagation characteristics of the planetary wave well and clearly represent the maintenance and development of the blocking high near the Ural Mountains and the deepening of the East Asian trough. However, because the model only focuses on the ISO components, the amplitude of the wave oscillation is relatively smaller than that of the ERA5 ground truth. From the perspective of RMSE and ACC, the prediction results of the SE-ResNet model over 10 days are superior to those of the CFSv2 model. In particular, after December 7, the contour lines of the CFSv2 model's prediction results near the Ural Mountains gradually become flat, and the position of the high-pressure ridge appears near 90° E, which is to the east of the real position. Compared with the ResNet model, the SE-ResNet model is only slightly worse at 12

https://doi.org/10.5194/gmd-2022-146
Preprint. Discussion started: 11 July 2022

UTC on December 7 and is better than the ResNet model at other times, with lower RMSE and larger ACC values.

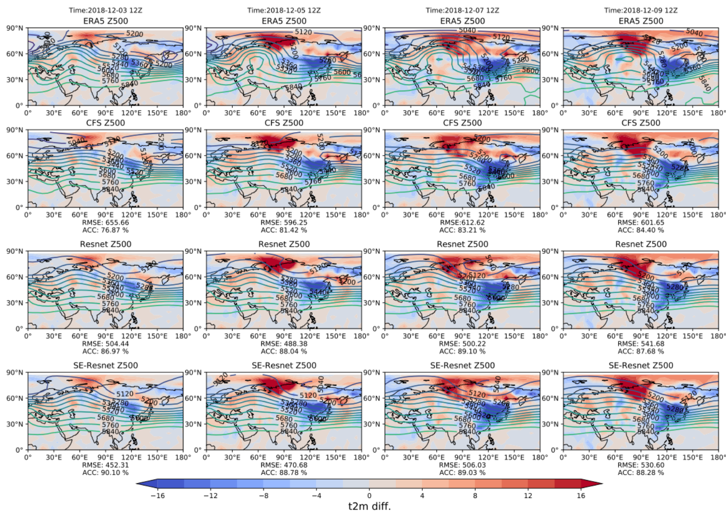

Figure 7. Comparison of different models' 500 hPa situation (unit: gpm) of a cold wave weather process in Eurasia (3-9 December 2018), and the difference (unit: K) of ERA5 ground 2 m temperature between the schematic time and 12 UTC on 2 December 2018. Forecast lead time is 10 days, 12 days, 14 days, and 16 days from left to right, respectively.

Turning now to the overall prediction effect of different models in the Eurasian region, the variation sequences of the averaged RMSE and ACC of the Z500 ISO components with the forecast lead times are shown in Fig. 8. It can be inferred that the SE-ResNet model performs best in the overall prediction of upper-level circulation over the Eurasian region. The averaged RMSE and ACC of 10-30 day are 578.72 m^2 s^{-2} and 83.85 %, respectively. The ResNet model is slightly worse than the SE-ResNet model, with a mean RMSE and ACC of 583.68 m^2 s^{-2} and 83.56 % for 10-30 day, respectively. The forecast skill of the CFSv2 model is lower than that of the deep learning model beyond 12 days, and the averaged RMSE and ACC at 10-30 day are 603.85 m^2 s^{-2} and 82.31 %, respectively. Similar to the global prediction results, RMSE and ACC predicted by CFSv2 show a large variation rate over 20 days, while it tends to be flat beyond that, with a smaller decrease rate over time.

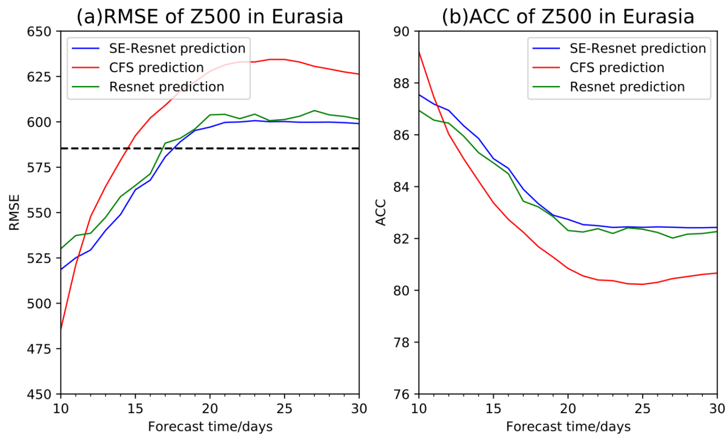

Figure 8. The prediction results of Z500 in the Eurasian region at different forecast lead times: (a) RMSE [m^2 s^{-2}], (b) ACC.

4. Discussion and Conclusions

In this paper, we used ISO components of atmospheric signals to train the SE-ResNet machine learning model to forecast the global Z500 and T850 situation in the next 1-30 day and compared the prediction results with the ResNet and CFSv2 models. Compared with the previous deep learning model, the forecast model used in this study has made the following important improvements. (1) As the prediction object gradually tends to become the low-frequency component with the increase in the forecast time within the subseasonal scale, the ISO components are directly used to train the forecast model. (2) Adding a self-attention mechanism optimizes the importance of different factor channels in the model.

We studied two indicators, RMSE and ACC, to evaluate the predictive performance of the model, and the results show that the SE-ResNet model is significantly better than the CFSv2 model in forecast lead times of 10-30 day. It is worth noting that the deep learning model is not endowed with meteorological constraints internally, but we still try to analyze the interpretability of its prediction results. The difference between the CFSv2 model and SE-ResNet model mainly occurs in the extratropical region and is small in the tropical region. Moreover, the SE-ResNet model has good performance in the prediction of planetary waves with wavenumbers of 3-8 beyond 11 days, which also leads to the difference in the prediction performance of the model in the extratropical regions. As an issue of focus, the variation characteristics of planetary waves are closely related to the occurrence and development process of weather. Not surprisingly, the data-driven model we developed in this study has a reliable reflection on the phase and propagation characteristics of planetary waves at forecast lead times of 11-30 day.

It should be noted that when latitude-weighted RMSE is used as the loss function training model in this paper, the predicted circulation oscillation features tend to be

https://doi.org/10.5194/gmd-2022-146
Preprint. Discussion started: 11 July 2022

smoothed over the forecast duration. For optimization of the model loss function, for example, the weight of the loss function increases with the forecast time, or the use of a multitime step loss function (Weyn et al., 2020) may help to improve the stability and accuracy of long-term prediction. On the other hand, meteorological elements are closely correlated with each other. Although deep learning provides a new method for the prediction of weather and climate evolution, the prediction objects in this study are limited to Z500 and T850 and are not necessarily constrained by the physical relationship between multiple elements (Kashinath et al., 2021), so using a machine learning framework based on physical models (e.g., Pawar et al., 2021; Karra et al., 2021) or combining dynamic models with deep learning models (e.g., He et al., 2021) may help improve the reliability and authenticity of subseasonal forecast models. Furthermore, recent studies have shown that probabilistic weather prediction makes it possible to calculate the uncertainty and skill index of neural network prediction (Clare et al., 2021), which also provides a reference basis for probabilistic prediction within the subseasonal timescale.

Appendix A

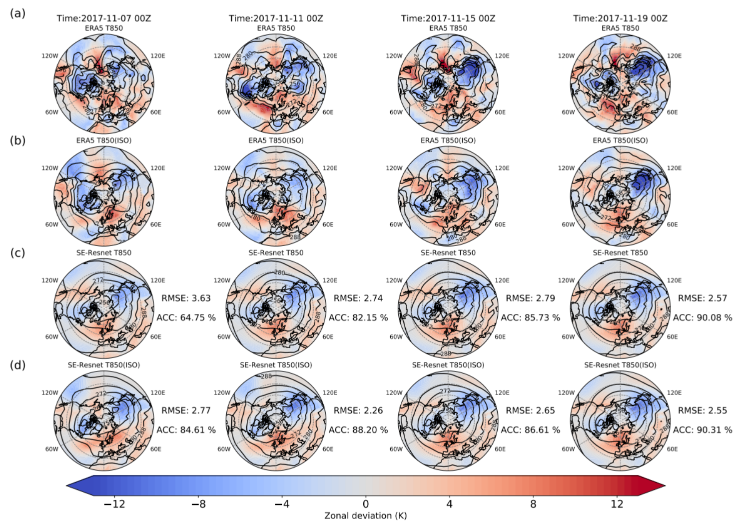

Figure A1. Result and zonal deviation comparison of model predictions for T850 (unit: K) in the Northern Hemisphere (20°-90° N, 180° W-180° E). Forecast lead times from left to right are 10 days, 14 days, 18 days and 22 days, respectively.

Code availability. The scripts for training the ResNet and SE-ResNet model, and constructing figures are available in the following Zenodo repository: https://zenodo.org/record/6592371 (Lu et al., 2022).

Data availability. The data for training the models and the prediction of the models are archived at https://zenodo.org/record/6592371 (Lu et al., 2022).

https://doi.org/10.5194/gmd-2022-146
Preprint. Discussion started: 11 July 2022

Author contributions. CL and DH conceived and designed the model, and verified the prediction effect of the model. CL, YS, and FX analysed the cases of this paper. CL and DH prepared the original draft of paper. YS and FX made further improvements to the manuscript.

Competing interests. The contact author has declared that neither they nor their co-authors have any competing interests.

Acknowledgements. The authors would like to thank the Center of Atmospheric Data Service, Nanjing University of Information Science & Technology, under the Geoscience Department of the National Natural Science Foundation of China, and the European Centre for Medium-Range Weather Forecasts for providing data.

Financial support. This work was supported jointly by the National Key Research and Development Program of China (grant number 2019YFC1510201) and the National Natural Science Foundation of China (grant number 41975073).

References

Clare, M. C., Jamil, O., and Morcrette, C.J.: Combining distribution-based neural networks to predict weather forecast probabilities, Quarterly Journal of the Royal Meteorological Society, 147, 4337-4357, https://doi.org/10.1002/qj.4180, 2021.

Hoskins, B. J.: The potential for skill across the range of the seamless weather - climate prediction problem: a stimulus for our science, Quarterly Journal of the Royal Meteorological Society, 139, 573-584, https://doi.org/10.1002/qj.1991, 2013.

Hong, S., Kim, S., Joh, M., and Song, S.: GlobeNet: Convolutional Neural Networks for Typhoon Eye Tracking from Remote Sensing Imagery, ArXiv, abs/1708.03417, 2017.

Ham, Y. G., Kim, J. H., and Luo, J. J.: Deep learning for multi-year enso forecasts, Nature, 573, 568-572, https://doi.org/10.1038/s41586-019-1559-7, 2019.

Hsu, P. C., Li, T., You, L., Gao, J., and Ren, H. L.: A spatial–temporal projection model for 10–30 day rainfall forecast in south china, Climate Dynamics, 44, 1227-1244, https://doi.org/10.1007/s00382-014-2215-4, 2015.

He, S., Li, X., Trenary, L., Cash, B. A., DelSole, T., and Banerjee, A.: Learning and dynamical models for sub-seasonal climate forecasting: comparison and collaboration, ArXiv, abs/2110.05196, 2021.

Hu, J., Shen, L., Albanie, S., Sun, G., and Wu, E.: Squeeze-and-Excitation Networks, IEEE Transactions on Pattern Analysis and Machine Intelligence, 42, 2011-2023, https://doi.org/10.1109/cvpr.2018.00745, 2020.

Jin, R., Ma, J., Ren, H., Yin, S., Cai, X., and Huang, W.: Advances and development countermeasures of 10～30 days extended-range forecasting technology in China, Advances in Earth Science, 34, 814-825, https://doi.org/10.11867/j.issn.1001-

https://doi.org/10.5194/gmd-2022-146
Preprint. Discussion started: 11 July 2022

8166.2019.08.0814, 2019.

Jin, W., Zhang, W., Hu, J., Weng, B., Huang, T., and Chen, J.: Using the Residual Network Module to Correct the Sub-Seasonal High Temperature Forecast, Frontiers in Earth Science, 9, https://doi.org/10.3389/feart.2021.760766, 2021.

Karra, S., Ahmmed, B., and Mudunuru, M. K.: AdjointNet: Constraining machine learning models with physics-based codes, ArXiv, abs/2109.03956, 2021.

Kashinath, K., Mustafa, M., Albert, A., Wu, J., Jiang, C., Esmaeilzadeh, S., Azizzadenesheli, K., Wang, R., Chattopadhyay, A., Singh, A., Manepalli, A., Chirila, D. B., Yu, R., Walters, R., White, B., Xiao, H., Tchelepi, H. A., Marcus, P. S., Anandkumar, A., Hassanzadeh, P., and Prabhat: Physics-informed machine learning: case studies for weather and climate modelling, Philosophical Transactions of the Royal Society A, 379, 20200093, https://doi.org/10.1098/rsta.2020.0093, 2021.

Li, W. , Hsu, P. C. , He, J. , Zhu, Z. , and Zhang, W.: Extended-range forecast of spring rainfall in southern china based on the madden–julian oscillation, Meteorology & Atmospheric Physics, 128, 331-345, https://doi.org/10.1007/s00703-015-0418-9, 2016.

Lu, C., Kong, Y., and Guan, Z.: A mask R-CNN model for reidentifying extratropical cyclones based on quasi-supervised thought, Scientific Reports, 10, 15011, https://doi.org/10.1038/s41598-020-71831-z, 2020.

Lagerquist, R., Allen, J. T., and McGovern, A.: Climatology and Variability of Warm and Cold Fronts over North America from 1979 to 2018, Journal of Climate, 33, 6531-6554, https://doi.org/10.1175/jcli-d-19-0680.1, 2020.

Lagerquist, R., Mcgovern, A., and Gagne, D. J.: Deep learning for spatially explicit prediction of synoptic-scale fronts, Weather and Forecasting, 34, 1137-1160, https://doi.org/10.1175/waf-d-18-0183.1, 2019.

Mayer, K. J., and Barnes, E. A.: Subseasonal Forecasts of Opportunity Identified by an Explainable Neural Network, Geophysical Research Letters, 48, e2020GL092092, https://doi.org /10.1029/2020GL092092, 2021.

Mathieu, M., Couprie, C., and LeCun, Y.: Deep multi-scale video prediction beyond mean square error, CoRR, abs/1511.05440, 2015.

Mohan, A., Livescu, D., Chertkov, M.: Wavelet-powered neural networks for turbulence, In ICLR 2020 Workshop on Climate Change AI, 2020.

Petoukhov, V., Rahmstorf, S., Petri, S., and Schellnhuber, H. J.: Quasiresonant amplification of planetary waves and recent Northern Hemisphere weather extremes, Proceedings of the National Academy of Sciences, 110, 5336-5341, https://doi.org/10.1073/pnas.1222000110, 2013.

Pawar, S., San, O., Nair, A. G., Rasheed, A., and Kvamsdal, T.: Model fusion with physics-guided machine learning: Projection-based reduced-order modeling, Physics of Fluids, 33, 067123, https://doi.org/10.1063/5.0053349, 2021.

Qi, X., Yang, J., Gao, M., Yang, H., and Liu, H.: Roles of the Tropical/Extratropical Intraseasonal Oscillations on Generating the Heat Wave Over Yangtze River Valley: A Numerical Study, Journal of Geophysical Research: Atmospheres, 124, 3110 –

https://doi.org/10.5194/gmd-2022-146
Preprint. Discussion started: 11 July 2022

Geoscientific Model Development
Open Access
Discussions

3123, https://doi.org/10.1029/2018jd029868, 2019.

Rasp, S., Dueben, P. D., Scher, S., Weyn, J. A., and Thuerey, N.: Weatherbench: a benchmark data set for data-driven weather forecasting, Journal of Advances in Modeling Earth Systems, 12, e2020MS002203, https://doi.org/10.1029/2020MS002203, 2020.

Rasp, S., Dueben, P. D., Scher, S., Weyn, J. A., and Thuerey, N.: Weatherbenh: a benchmark data set for data-driven weather forecasting, TUM [data set], https://mediatum.ub.tum.de/1524895, 2020.

Robertson, A. W., Kumar, A., Peña, M., and Vitart, F.: Improving and Promoting Subseasonal to Seasonal Prediction, Bulletin of the American Meteorological Society, 96(3), ES49-ES53, https://doi.org/10.1175/bams-d-14-00139.1, 2015.

Rasp, S., and Thuerey, N.: Data-driven medium-range weather prediction with a resnet pretrained on climate simulations: A new model for weatherbench, Journal of Advances in Modeling Earth Systems, 13, e2020MS002405, https://doi.org/10.1029/2020MS002405, 2021.

Rasp, S., and Thuerey, N.: Data-driven medium-range weather prediction with a resnet pretrained on climate simulations: A new model for weatherbench, Github [code], https://github.com/raspstephan/WeatherBench, 2021.

Slingo, J. M., Bates, K. R., Nikiforakis, N., Piggott, M. D., Roberts, M. J., Shaffrey, L. C., Stevens, I. T., Vidale, P. L., and Weller, H.: Developing the next-generation climate system models: challenges and achievements, Philosophical Transactions of the Royal Society A: Mathematical, Physical and Engineering Sciences, 367, 815-831, https://doi.org/10.1098/rsta.2008.0207, 2008.

Shi, X., Chen, Z., Wang, H., Yeung, D., Wong, W., and Woo, W.: Convolutional LSTM Network: A Machine Learning Approach for Precipitation Nowcasting, NIPS, https://doi.org/10.5555/2969239.2969329, 2015.

Sønderby, C. K., Espeholt, L., Heek, J., Dehghani, M., Oliver, A., Salimans, T., Agrawal, S., Hickey, J., and Kalchbrenner, N.: MetNet: A Neural Weather Model for Precipitation Forecasting, ArXiv, abs/2003.12140, 2020.

Srinivasan, V., Khim, J., Banerjee, A., and Ravikumar, P.: Subseasonal climate prediction in the western US using Bayesian spatial models, UAI, 2021.

Screen, J. A., and Simmonds, I.: Amplified mid-latitude planetary waves favour particular regional weather extremes, Nature Climate Change, 4, 704-709, https://doi.org/10.1038/nclimate2271, 2014.

Song, K., Yu, X., Gu, Z., Zhang, W., Yang, G., Wang, Q., Xu, C., Liu, J., Liu, W., Shi, C., Wang, Y., and Zhang, G.: Deep Learning Prediction of Incoming Rainfalls: An Operational Service for the City of Beijing China, 2019 International Conference on Data Mining Workshops (ICDMW), 180-185, https://doi.org/10.1109/icdmw.2019.00036, 2019.

Vitart, F., Ardilouze, C., Bonet, A., Brookshaw, A. M., Chen, M., Codorean, C., Déqué, M., Ferranti, L., Fucile, E., Fuentes, M., Hendon, H. H., Hodgson, J., Kang, H., Kumar, A., Lin, H., Liu, G., Liu, X., Malguzzi, P., Mallas, I., Manoussakis, M. N.,

https://doi.org/10.5194/gmd-2022-146
Preprint. Discussion started: 11 July 2022

Geoscientific Model Development Discussions

Mastrangelo, D., MacLachlan, C., McLean, P., Minami, A., Mládek, R., Nakazawa, T., Najm, S. K., Nie, Y., Rixen, M., Robertson, A. W., Ruti, P. M., Sun, C., Takaya, Y., Tolstykh, M. A., Venuti, F., Waliser, D. E., Woolnough, S. J., Wu, T., Won, D. J., Xiao, H., Zaripov, R. B., and Zhang, L.: The Subseasonal to Seasonal (S2S) Prediction Project Database, Bulletin of the American Meteorological Society, 98, 163-173, 2017.

Wang, Q., Chou, J., and Feng, G.: Extracting predictable components and forecasting techniques in extended-range numerical weather prediction, Science China Earth Sciences, 57, 1525-1537, https://doi.org/10.1007/s11430-014-4832-5, 2014.

Weyn, J. A., Durran, D. R., and Caruana, R.: Can machines learn to predict weather? Using deep learning to predict gridded 500hPa geopotential height from historical weather data, Journal of Advances in Modeling Earth Systems, 11, 2680–2693, https://doi.org/10.1029/2019MS001705, 2019.

Weyn, J. A., Durran, D. R., and Caruana, R.: Improving data-driven global weather prediction using deep convolutional neural networks on a cubed sphere, Journal of Advances in Modeling Earth Systems, 12, e2020MS002109, https://doi.org/10.1029/2020MS002109, 2020.

Weyn, J. A., Durran, D. R., Caruana, R., and Cresswell-Clay, N.: Sub-seasonal forecasting with a large ensemble of deep-learning weather prediction models, Journal of Advances in Modeling Earth Systems, 13, e2021MS002502, https://doi.org/10.1029/2021MS002502, 2021.

Wu, J., Kashinath, K., Albert, A., Chirila, D.B., Prabhat, and Xiao, H.: Enforcing statistical constraints in generative adversarial networks for modeling chaotic dynamical systems, J. Comput. Phys., 406, 109209, https://doi.org/10.1016/j.jcp.2019.109209, 2020.

Zhu, Z. , Li, T. , Bai, L. , and Gao, J.: Extended-range forecast for the temporal distribution of clustering tropical cyclogenesis over the western north pacific, Theoretical and Applied Climatology, 130, 865-877, https://doi.org/10.1007/s00704-016-1925-4, 2017.

Zhu, H., Wheeler, M. C., Sobel, A. H., and Hudson, D.: Seamless precipitation prediction skill in the tropics and extratropics from a global model, Monthly Weather Review, 142, 1556-1569, https://doi.org/10.1175/mwr-d-13-00222.1, 2014.

Zhang, D., Zheng, Z., Chen, L., and Zhang, P.: Advances on the Predictability and Prediction Methods of 10-30 d Extended Range Forecast, Journal of Applied Meteorological Science, 30: 416-430, https://doi.org/10.11898/1001-7313.20190403, 2019.